NONLINEAR DYNAMIC ANALYSIS FOR FGM CIRCULAR PLATES

H.-L. Dai * **X. Yan** **L. Yang**

State Key Laboratory of Advanced Design and Manufacturing for Vehicle Body
Hunan University
Changsha, 410082, China

Department of Engineering Mechanics, College of Mechanical & Vehicle Engineering,
Hunan University
Changsha, 410082, China

ABSTRACT

In the paper, nonlinear dynamic analysis of a circular plate composed of functionally graded material (FGM) is presented. Considering a transverse shear deformation and geometric nonlinearity, the von Karman geometric relation of the FGM circular plate is established. Based on the theory of the first-order shear deformation, a new set of equilibrium equations is developed by the principle of minimum total energy. Applying the finite difference method and Newmark scheme, the nonlinear transient problem is solved by the iterative method. To validate the presented method, the transient problem of the FGM circular plate is compared with those of the existed literature, and good agreement is observed. The effects of the volume fraction index, boundary conditions, mechanical load and the ratio of thickness to radius on the nonlinear transient problem of the FGM circular plate are investigated.

Keywords: Nonlinear, Dynamic analysis, FGM circular plate.

1. INTRODUCTION

Circular plates composed of functionally graded materials (FGMs) are widely used in aerospace, nuclear reactors, internal combustion engines and other fields. However, these FGM circular plates, often under severe conditions, would exhibit obvious creep buckling property within the serving time due to its intrinsic viscoelastic property. Therefore, dynamic analysis of a FGM circular plate is very important.

In recent years, extensive investigations on the mechanical behaviors of FGM circular plates were carried out by many authors. Ma and Wang [1] investigated axisymmetric large deflection bending of a FGM circular plate under thermal and mechanical loadings. Based on the Love–Kirchhoff hypothesis, Najafizadeh *et al*. [2,3] analyzed buckling behaviors of FGM circular plates. Based on the classical plate theory, Ehrahimi and Rastgo [4] presented analytical investigation on the free vibration behavior of thin FGM circular plates integrated with two uniformly distributed actuator layers made of piezoelectric material. Li *et al.* [5] considered the bending of transversely isotropic circular plates with elastic compliance coefficients being arbitrary functions of the thickness coordinate, subject to a transverse load. Based on the unconstrained third-order shear deformation plate theory, axisymmetric bending and buckling of perfect functionally graded solid circular plates are studied by Saidi *et al*. [6]. Resting on the Pasternak elastic foundation, Hosseini *et al*. [7] investigated buckling and free vibration behaviors of radially functionally graded circular and annular sector thin plates subjected to uniform in-plane compressive loads. Based on the three-dimensional elastic theory, Nie and Zhong [8] achieved dynamic analysis of multi-directional FGM annular plates by using a semi-analytical numerical method. Based on Kirchhoff's–Love hypothesis, Ebrahimi and Rastgoo [9] presented a theoretical model for geometrically nonlinear vibration analysis of FGM circular plates. By means of the differential transformation method, Shariyat and Alipour [10] developed a semi-analytical solution for free vibration and modal stress analyses of two-dimensional FGM circular plates resting on two-parameter elastic foundations. Recently, Shariyat and Jafari [11] presented nonlinear low- velocity impact analysis of two-directionally graded circular plates under radial preloads. Khorshidvand *et al*. [12] studied thermal buckling of FGM circular plates with surface-bounded piezoelectric layers. Li *et al*. [13] presented a set of axisymmetric analytical solutions of the thermo- elasticity field induced by the external thermal load, in a heterogeneous circular plate. To the authors' knowledge, the nonlinear dynamic analysis of a FGM circular plate has not been carried out in the previous works.

In the present paper, nonlinear dynamic analysis of a FGM circular plate is presented. Considering a transverse shear deformation and geometric nonlinearity, the

* Corresponding author (hldai520@sina.com)

DOI : 10.1017/jmech.2012.139
Copyright © 2013 The Society of Theoretical and Applied Mechanics, R.O.C.
https://doi.org/10.1017/jmech.2012.139 Published online by Cambridge University Press

von Karman geometric relation of the FGM circular plate is established. Based on the theory of the first-order shear deformation, a new set of equilibrium equations is developed by the principle of minimum total energy. Applying the finite difference method and Newmark scheme, the nonlinear transient problem is solved by the iterative method.

2. FORMULATION OF THE PROBLEM

Consider a FGM circular plate subjected to an axisymmetric transverse load with thickness h and radius of a as shown in Fig. 1. The cylindrical coordinate system (r, θ, z) is set on the mid-plane (z = 0), located at its initially undeformed configuration. The r-coordinate direction is radially outward from the center of the circular plate, the θ-coordinate is directed along the circumference and the z-coordinate along the thickness of the circular plate. In this paper, the bottom and top surfaces of the FGM circular plate are made of metal and ceramic materials, respectively.

2.1 Material Properties of a Viscoelastic FGM

Material properties P (*e.g.*, Young's modulus E and mass density ρ) of the FGM circular plate are assumed to vary through the thickness of the plate, as a function of the volume fraction and properties of the constituent materials. Material properties can be expressed as (Woo and Meguid, [14])

$$P = P_c V_c + P_m V_m \tag{1}$$

where V_c and V_m are the volume fraction of metal and ceramic materials, respectively, P_c and P_m are material properties of metal and ceramic materials, respectively.

The volume fraction V_c and V_m should add up to one

$$V_c + V_m = 1 \tag{2}$$

The volume fraction V_c can be written as (Reddy, [15])

$$V_c(z) = \left(\frac{2z+h}{2h}\right)^n \tag{3}$$

The volume fraction index n dictates the material variation profile across the thickness of the viscoelastic FGM circular plate, from Eqs. (1) ~ (3), gives

$$P(z) = (P_c - P_m)\left(\frac{2z+h}{2h}\right)^n + P_m \tag{4}$$

The Poisson ratio v is considered to be constant along the thickness of the FGM circular plate.

In the present research, the viscoelastic property is also assumed to be varying along the thickness of the FGM circular plate, and the ceramic relaxation coefficient δ_c is considered to be zero, that is to say, the viscoelastic property of the ceramic material is neglected. Therefore, the relaxation coefficient δ of the FGM circular plate may be expressed as

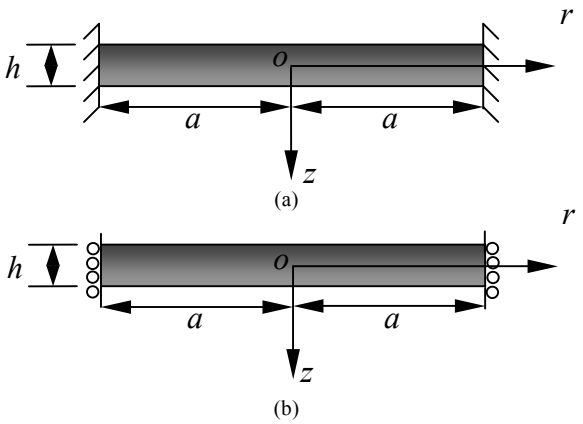


Fig. 1 Sketch map of a FGM circular plate, (a) with clampled boundary conditions; (b) with simply supported boundary conditions

$$\delta(z) = \left(1 - V_c(z)\right)\ \delta_m \tag{5}$$

where δ_m denotes the relaxation coefficient of metal material.

2.2 Governing Equations

The first-order shear deformation plate theory (FST) is the simplest theory that accounts for nonzero transverse shear strain, the displacement field of the FGM circular plate may be expressed as

$$u_r(r,\ z,\ t) = u(r,\ t) + z\varphi(r,\ t) \tag{6a}$$

$$u_z(r,\ z,\ t) = w(r,\ t) \tag{6b}$$

where u_r and u_z are the radial and transverse displacements of the FGM circular plate, respectively, and $u(r, t)$ and $w(r, t)$ are the radial and transverse displacements of the point on the middle surface of the FGM circular plate, respectively. $\varphi(r, t)$ denotes rotation of a transverse normal in the plane θ.

In accordance with these assumptions, the strains at any level z from the middle surface of the FGM circular plate are obtained by (Reddy and Huang, [16])

$$\varepsilon_r = u_{,r} + \frac{1}{2}(w_{,r})^2 + z\varphi_{,r} \tag{7a}$$

$$\varepsilon_\theta = \frac{u}{r} + z\frac{1}{r}\varphi \tag{7b}$$

$$\varepsilon_{rz} = w_{,r} + \varphi \tag{7c}$$

where ε_r, ε_θ and ε_{rz} are strains along the r and θ directions and rz plane, respectively, the subscript comma denotes differentiation with respect to r. Considering linear viscoelastic stress-strain relation of the FGM circular plate, the following relation can be obtained by applying the Boltzmann superposition theory

$$\sigma_r = C_{11} \otimes \varepsilon_r + C_{12} \otimes \varepsilon_\theta \tag{8a}$$

$$\sigma_\theta = C_{21} \otimes \varepsilon_r + C_{22} \otimes \varepsilon_\theta \tag{8b}$$

https://doi.org/10.1017/jmech.2012.139 Published online by Cambridge University Press

$$\sigma_{rz} = C_{55} \otimes \varepsilon_{rz} \tag{8c}$$

where $C_{11} = C_{22} = E(z)/1-\nu^2$, $C_{12} = C_{21} = \nu E(z)/1-\nu^2$ and $C_{55} = E(z)/2(1+\nu)$, "$\otimes$"is the Stieltjes convolution sign and defined as

$$\begin{aligned} & C_{11}(t) \otimes \varepsilon_r(t) \\ & = C_{11}(0)\ \varepsilon_r(t) + C_{11}(t)_{,t}\, \varepsilon_r(t) \\ & = C_{11}(0)\ \varepsilon_r(t) + \int_0^t C_{11}(t-\tau)_{,\tau} \varepsilon_r(\tau)\, d\tau \end{aligned} \tag{9}$$

The membrane forces, bending moments and shearing force are, respectively, expressed as follows

$$(N_r,\ N_\theta) = \int_{-h/2}^{h/2} (\sigma_r,\ \sigma_\theta)\ dz \tag{10a}$$

$$(M_r,\ M_\theta) = \int_{-h/2}^{h/2} (\sigma_r,\ \sigma_\theta)\ z dz \tag{10b}$$

$$Q_r = K \int_{-h/2}^{h/2} \sigma_{rz}\ dz \tag{10c}$$

For simplicity, let

$$\begin{aligned} & \varepsilon_r^0 = u_{,r} + \frac{1}{2}(w_{,r})^2 \ , \ \ \varepsilon_\theta^0 = \frac{u}{r} \ , \ \ \varepsilon_{rz}^0 = w_{,r} + \varphi \ , \\ & \kappa_1 = \varphi_{,r} \ , \ \ \kappa_2 = \frac{\varphi}{r} \end{aligned} \tag{11}$$

Substituting Eqs. (8) and (11) into Eq. (10), yields

$$N_r = A_{11} \otimes \varepsilon_r^0 + A_{12} \otimes \varepsilon_\theta^0 + B_{11} \otimes \kappa_1 + B_{12} \otimes \kappa_2 \tag{12a}$$

$$N_\theta = A_{21} \otimes \varepsilon_r^0 + A_{22} \otimes \varepsilon_\theta^0 + B_{21} \otimes \kappa_1 + B_{22} \otimes \kappa_2 \tag{12b}$$

$$M_r = B_{11} \otimes \varepsilon_r^0 + B_{12} \otimes \varepsilon_\theta^0 + D_{11} \otimes \kappa_1 + D_{12} \otimes \kappa_2 \tag{12c}$$

$$M_\theta = B_{21} \otimes \varepsilon_r^0 + B_{22} \otimes \varepsilon_\theta^0 + D_{21} \otimes \kappa_1 + D_{22} \otimes \kappa_2 \tag{12d}$$

$$Q_r = KA_{55} \otimes \varepsilon_{rz}^0 \tag{12e}$$

where $A_{ij} = \int_{-h/2}^{h/2} C_{ij}\ dz$, $B_{ij} = \int_{-h/2}^{h/2} C_{ij}\ z dz$, $D_{ij} = \int_{-h/2}^{h/2} C_{ij}\ z^2 dz$ $(i = j = 1,\ 2,\ 5)$ and K is the shear correction factor, and K = 5/6 (Reddy and Huang, [16]; Reddy *et al*. [17]).

In accordance with the principle of minimum total energy (Bayat, [18]), $\delta\Pi = 0$ implies

$$\begin{aligned} & \int_0^r \left(\left(N_\theta - \frac{d}{dr}(rN_r) \right) \delta u + \left(M_\theta + rQ_r - \frac{d}{dr}(rM_r) \right) \delta\varphi \right) dr \\ & - \int_0^r \left(\frac{d}{dr}\left(rQ_r + rN_r \frac{dw}{dr} \right) + rq(r,t) \right) \delta w dr = 0 \end{aligned} \tag{13}$$

where $q(r, t)$ is a transverse mechanical load.

The nonlinear governing equations can be expressed as follows

$$N_{r,r} + \frac{1}{r}(N_r - N_\theta) = 0 \tag{14a}$$

$$M_{r,r} + \frac{M_r - M_\theta}{r} = Q_r \tag{14b}$$

$$(rQ_r)_{,r} + (rN_r\ w_{,r})_{,r} + rq(r,\ t) = \int_{-h/2}^{h/2} \rho dz r w_{,tt} \tag{14c}$$

Substituting Eqs. (12) into Eqs. (14a ~ 14c), the nonlinear viscoelastic governing equations of the FGM circular plate can be obtained as

$$\begin{aligned} & A_{11} \otimes \left(u_{,rr} r + r w_{,r} w_{,rr} + u_{,r} + \frac{1}{2} w_{,r} w_{,r} \right) + A_{12} \otimes u_{,r} + B_{12} \otimes \varphi_{,r} \\ & + B_{11} \otimes (\varphi_{,rr}\ r + \varphi_{,r}) - A_{21} \otimes \left(u_{,r} + \frac{1}{2} w_{,r}\ w_{,r} \right) \\ & - A_{22} \otimes \frac{u}{r} - B_{22} \otimes \frac{\varphi}{r} - B_{21} \otimes \varphi_{,r} = 0 \end{aligned} \tag{15a}$$

$$\begin{aligned} & B_{11} \otimes \left(u_{,rr} r + r w_{,r} w_{,rr} + u_{,r} + \frac{1}{2} w_{,r} w_{,r} \right) + B_{12} \otimes u_{,r} + D_{12} \otimes \varphi_{,r} \\ & + D_{11} \otimes (\varphi_{,rr}\ r + \varphi_{,r}) - B_{21} \otimes \left(u_{,r} + \frac{1}{2} w_{,r}\ w_{,r} \right) - B_{22} \otimes \frac{u}{r} \\ & - D_{22} \otimes \frac{\varphi}{r} - D_{21} \otimes \varphi_{,r} - KA_{55} \otimes (\varphi r + r w_{,r}) = 0 \end{aligned} \tag{15b}$$

$$\begin{aligned} & KA_{55} \otimes (r\varphi_{,r} + r w_{,rr} + \varphi + w_{,r}) + \left(A_{11} \otimes (u_{,rr} + w_{,r} w_{,rr}) \right. \\ & + A_{12} \otimes \left(\frac{u_{,r}}{r} - \frac{u}{r^2} \right) + B_{12} \otimes \left(\frac{\varphi_{,r}}{r} - \frac{\varphi}{r^2} \right) + B_{11} \otimes \varphi_{,rr} \Big) (r w_{,r}) \\ & + \left(A_{11} \otimes (u_{,r} + \frac{1}{2} w_{,r} w_{,r}) + A_{12} \otimes \frac{u}{r} + B_{12} \otimes \frac{\varphi}{r} \right. \\ & \left. + B_{11} \otimes \varphi_{,r} \right) (w_{,r} + r w_{,rr}) + rq(r,\ t) - \bar{\rho} r w_{,tt} = 0 \end{aligned} \tag{15c}$$

where $\bar{\rho} = \int_{-h/2}^{h/2} \rho dz$. Eqs. (15a ~ 15c) are integro-partial differential equations, and the relaxation modulus of the FGM circular plate in both time and space dependent, so it is impossible to obtain an numerical solution to this problem.

The conditions at the center of the FGM circular plate is expressed as

$$\varphi = w_{,r} = u = 0 \ , \ \ \text{at} \ \ r = 0 \tag{16}$$

Here, two kinds of boundary condition are considered in the case 1 and case 2.

Case 1. The clamped boundary conditions

$$\varphi = w = w_{,r} = u = 0 \ , \ \text{at} \ \ r = a \tag{17}$$

Case 2. The simply supported boundary conditions

$$M_r = w = u = 0 \ , \ \text{at} \ \ r = a \tag{18}$$

https://doi.org/10.1017/jmech.2012.139 Published online by Cambridge University Press

3. SOLUTION'S METHODOLOGY

In order to get the solution to the governing Eqs. (15a ~ 15c), the displacements u, w and φ in space domain are separated by the finite difference method and in time domain are discrete by the Newton-Newmark method. Currently, the most widely used material of a descriptive model of viscoelastic behavior is to expand its relaxation modulus into the Prony-dirichlet series form, and the relaxation modulus in the equations can be expanded as (Fu *et al*., [19])

$$E(z,\ t) = E(z) + \sum_{i=1}^{\chi} E_i(z)\ e^{-\delta_i(z)t} \tag{19}$$

where χ is the number of the terms to be expanded, $E(z)$, $E_i(z)$ and $\delta i(z)$ are material parameters, respectively. If $\chi = 1$, the material is a standard linear solid.

Considering the generality, the $E(t)$ represents A_{ij}, B_{ij}, D_{ij} and f refers to the unknown displacement variables (u, w, φ). There are similar items to $E(t)\otimes f(r,\ t)$, $E(t)\otimes f(r,t)f(r,t)$, $\left[E(t)\otimes f(r,\ t)\right]f(r,\ t)$, $\left[E(t)\otimes f(r,\ t)f(r,\ t)\right]f(r,\ t)$ in the governing equations and boundary conditions. Below these items will be calculated, respectively.

The FGM circular plate is set as a standard linear solid in the present model. Dividing the time t equally into small time segments Δt, and $t = \lambda\Delta t$. Then, gives

$$\begin{aligned} &E(t)\otimes f(r,\ t) = (E_0 + E_1)f(r,\ t) \\ &-\delta_1 E_1 e^{-\delta_1 t}\left[\int_0^{\Delta t} e^{\delta_1\tau} f(r,\ \tau)\ d\tau\right. \\ &\left.+\int_{\Delta\tau}^{2\Delta t} e^{\delta_1\tau} f(r,\ \tau)\ d\tau + \cdots + \int_{(\lambda-1)\Delta\tau}^{\lambda\Delta t} e^{\delta_1\tau} f(r,\ \tau)\ d\tau\right] \end{aligned} \tag{20}$$

Because Δt is small, Eq. (20) can be expanded with adoption of the Newton-Cotes trapezoidal formula.

$$\begin{aligned} &E(t)\otimes f(r,\ t) = (E_0 + E_1)f(r,\ t) \\ &-\delta_1\ E_1\ e^{-\delta_1 t}\left[\frac{\Delta t}{2}\left(f(r,\ 0) + e^{\delta_1\Delta t} f(r,\ \Delta t)\right.\right. \\ &+e^{\delta_1\Delta t} f(r,\ \Delta t) + e^{2\delta_1\Delta t} f(r,\ 2\Delta t) + \cdots \\ &\left.\left.+e^{(\lambda-1)\delta_1\Delta t} f\left(r,(\lambda-1)\Delta t\right) + e^{\lambda\delta_1\Delta\tau} f(r,\ \lambda\Delta t)\right)\right] \end{aligned} \tag{21}$$

For the convenience of calculation, Eq. (21) is rewritten as

$$\begin{aligned} &E(t)\otimes f(r,\ t) = (E_0 + E_1)f(r,\ \lambda\Delta t) \\ &-\frac{\Delta t}{2}\delta_1\ E_1\ e^{-\delta_1\lambda\Delta t}\left[f(r,\ 0) + e^{\delta_1\lambda\Delta t} f(r,\ \lambda\Delta t)\right. \\ &\left.+2\sum_{K=1}^{\lambda-1} e^{\delta_1 K\Delta t} f(r,\ K\Delta t)\right] \\ &= (E_0 + E_1 + \Delta t\delta_1\ E_1)f(r,\ \lambda\Delta t) \\ &\quad -\frac{\Delta t}{2}\delta_1 E_1\ e^{-\delta_1\lambda\Delta t}\left[(f(r,\ 0) + 2\sum_{K=1}^{\lambda-1} e^{\delta_1 K\Delta t} f(r,\ K\Delta t)\right] \end{aligned} \tag{22}$$

In each iterative step j, the nonlinear items in the equations and the boundary equations can be linearized in the following way

$$(x,\ y)_j = (x)_j (y)_{jp} \tag{23}$$

where $(y)_{jp}$ is the average value of those obtained in previous two iterations. For the initial iterative step, it can be determined by using the quadratic extrapolation, *i.e.*

$$(y)_{jp} = A(y)_{j-1} + B(y)_{j-2} + C(y)_{j-3} \tag{24}$$

and for different iterative steps, the coefficients A, B and C can be expressed as follows

$$j = 1 : A = 1\ ,\ \ B = 0\ ,\ \ C = 0 \tag{25a}$$

$$j = 2 : A = 2\ ,\ \ B = -1\ ,\ \ C = 0 \tag{25b}$$

$$j \geq 3 : A = 3\ ,\ \ B = -3\ ,\ \ C = 1 \tag{25c}$$

Using the same method, the other items can be expressed as

$$\begin{aligned} &E(t)\otimes f(r,\ t)f(r,\ t) = (E_0 + E_1)f(r,\ \lambda\Delta t)f(r)_{jp} \\ &-\frac{\Delta t}{2}\delta_1\ E_1\ e^{-\delta_1\lambda\Delta t}\times\left[(f(r,0)f(r)_{jp} + e^{\delta_1\lambda\Delta t} f(r,\lambda\Delta t)f(r)_{jp}\right. \\ &\left.+2\sum_{K=1}^{\lambda-1} e^{\delta_1 K\Delta t} f(r,\ K\Delta t)f(r)_{jp}\right] \\ &= (E_0 + E_1 + \Delta t\delta_1 E_1)f(r,\ \lambda\Delta t)f(r)_{jp} \\ &-\frac{\Delta t}{2}\delta_1 E_1\ e^{-\delta_1\lambda\Delta t}\left[(f(r,0)f(r)_{jp} + 2\sum_{K=1}^{\lambda-1} e^{\delta_1 K\Delta t} f(r,K\Delta t)f(r)_{jp}\right] \end{aligned} \tag{26a}$$

$$\begin{aligned} &\left(E(t)\otimes f(r,\ t)\right)f(r,\ t) = \left\{(E_0 + E_1)f(r)_{jp}\right. \\ &-\frac{\Delta t}{2}\delta_1 E_1\ e^{-\delta_1\lambda\Delta t}\left[f(r)_{jp} + e^{\delta_1\lambda\Delta t} f(r)_{jp}\right. \\ &\left.\left.+2\sum_{K=1}^{\lambda-1} e^{\delta_1 K\Delta t} f(r)_{jp}\right]\right\} f(r,\ \lambda\Delta t) = \left\{(E_0 + E_1 + \Delta t\delta_1 E_1)f(r)_{jp}\right. \\ &\left.-\frac{\Delta t}{2}\delta_1 E_1 e^{-\delta_1\lambda\Delta t}\left[f(r)_{jp} + 2\sum_{K=1}^{\lambda-1} e^{\delta_1 K\Delta t} f(r)_{jp}\right]\right\} f(r,\ \lambda\Delta t) \end{aligned} \tag{26b}$$

$$\begin{aligned} &\left(E(t)\otimes f(r,\ t)f(r,\ t)\right)f(r,\ t) = \left\{(E_0 + E_1)f(r)_{jp} f(r)_{jp}\right. \\ &-\frac{\Delta t}{2}\delta_1 E_1\ e^{-\delta_1\lambda\Delta t}\left[f(r)_{jp} f(r)_{jp} + e^{\delta_1\lambda\Delta t} f(r)_{jp} f(r)_{jp}\right. \\ &\left.\left.+2\sum_{K=1}^{\lambda-1} e^{\delta_1 K\Delta t} f(r)_{jp} f(r)_{jp}\right]\right\} f(r,\ \lambda\Delta t) \\ &= \left\{(E_0 + E_1 + \Delta t\delta_1 E_1)f(r)_{jp} f(r)_{jp}\right. \\ &-\frac{\Delta t}{2}\delta_1 E_1 e^{-\delta_1\lambda\Delta t}\left[f(r)_{jp} f(r)_{jp}\right. \\ &\left.\left.+2\sum_{K=1}^{\lambda-1} e^{\delta_1 K\Delta t} f(r)_{jp} f(r)_{jp}\right]\right\} f(r,\ \lambda\Delta t) \end{aligned} \tag{26c}$$

Applying the Newmark assumption, $w_{,t}$ and w can be obtained at $t + \Delta t$

https://doi.org/10.1017/jmech.2012.139 Published online by Cambridge University Press

$$(w_{,t})_j = \Delta t\left(\zeta(w_{,tt})_j + (1-\zeta)(w_{,tt})_{j-1}\right) + (w_{,t})_{j-1} \tag{27a}$$

$$(w)_j = (w)_{j-1} + \Delta t(w_{,t})_{j-1} + \left(\xi(w_{,tt})_j + \left(\frac{1}{2}-\xi\right)(w_{,tt})_{j-1}\right)(\Delta t)^2 \tag{27b}$$

where the parameters ζ and ξ can be determined by integration accuracy and stability. From Eq. (27b), yields

$$(w_{,tt})_j = \frac{\left((w)_j - (w)_{j-1}\right)}{\xi(\Delta t)^2} - \frac{(w_{,t})_{j-1}}{\xi(\Delta t)} - \left(\frac{1}{2\xi}-1\right)(w_{,tt})_{j-1} \tag{28}$$

when $\zeta = 1/2$ and $\xi = 1/4$, this is the average acceleration method. Into the above-mentioned treatment, the governing equations and boundary equations can be transformed into a series of linear equation at each discrete point, and the solution to these linear equations can be acquired. For each iteration step, the iterations last until the difference of the present value and the former step's value is smaller than 10^{-3}, the convergent solution in j step is presented, and the entire iterative will end.

4. NUMERICAL RESULTS AND DISCUSSION

4.1 The Transient Response of the FGM Circular Plate

To ensure the validity and accuracy of the present method, the present model is degenerated into a clamped FGM circular plate. w_0 represents the center deflection of the FGM circular plate, and $\overline{w} = 64w_0 D_0 / q \times a^4$ represents the non-dimensional deflection of the FGM circular plate. Material parameters are selected as the same as a reference (Reddy *et al.* [17]). Comparison of the results by the present model with that of the reference is presented in Table 1. From Table 1, good agreement is presented, and it is clear that the present method is correct.

4.2 The Bending Deformation of the Viscoelastic FGM Circular Plate

Consider a FGM circular plate with the clamped and simply support boundary conditions subjected to an axisymmetric transverse load $q = 100 \times 10^6$Pa. In the section, material parameters are taken as

$$\nu = 0.3,\ E_m = (1+9\times e^{-\delta_1 t})\ \text{GPa},\ \rho_m = 5600\text{kg/m}^3,$$
$$\delta = 0.2,\ E_c = 200\times 10^9\, Pa,\ \rho_c = 7800\text{kg/m}^3 \tag{29}$$

Figure 2 shows the change of Young's modulus for the FGM circular plate at the different thickness. From the curves of the Fig. 2, it is seen that the Young's modulus increases from the up surface to the bottom surface of the FGM circular plate at the same time point, and the amplitude of Young's modulus arrives at a certain stable value as the time increases.

Table 1 Non-dimensional deflection of clamped FGM circular plates

n	The ratio of thickness to radius, h/a					
	0.05		0.1		0.15	
	Reddy *et al.* [17]	This paper	Reddy *et al.* [17]	This paper	Reddy *et al.* [17]	This paper
0	2.554	2.392	2.639	2.633	2.781	2.778
2	1.402	1.361	1.444	1.441	1.515	1.513
4	1.282	1.248	1.320	1.317	1.384	1.382
6	1.220	1.190	1.257	1.254	1.318	1.317
8	1.181	1.154	1.217	1.215	1.278	1.276
10	1.155	1.129	1.190	1.188	1.250	1.248
15	1.114	1.091	1.149	1.147	1.208	1.206
20	1.092	1.069	1.126	1.124	1.184	1.183
25	1.077	1.056	1.112	1.109	1.169	1.168
30	1.067	1.046	1.101	1.099	1.159	1.157
35	1.060	1.039	1.094	1.091	1.151	1.150
40	1.054	1.034	1.088	1.086	1.145	1.144
50	1.046	1.026	1.080	1.078	1.137	1.136
10^2	1.029	1.010	1.063	1.061	1.119	1.118
10^3	1.013	0.995	1.047	1.045	1.103	1.102
10^4	1.011	1.000	1.045	1.043	1.101	1.100
10^5	1.011	1.000	1.045	1.043	1.101	1.100

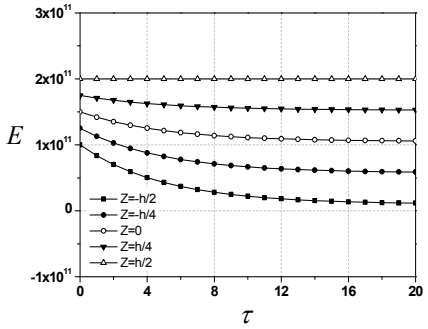


Fig. 2 The changes of Young's modulus E of the FGM circular plate with time at various thicknesses

Figure 3 shows the change of the center deflection for the FGM circular plate with different volume fractions V_c at the clamped and simply supported boundary conditions. From Fig. 3(a), it is seen that the center deflection of the FGM circular plate increases as the time increases, and it arrives at a stable value at a certain time values which is longer as the V_c decreases. It is also seen from the figure that the center deflection of the structure decreases as the V_c increases at the same time point. Comparing Fig. 3(a) with Fig. 3(b), the change of center deflection for the FGM circular plate with two types of boundary conditions is similar, the magnitudes of deflection for the FGM circular plate at the clamped boundary conditions is smaller than those of the FGM circular plate at the simply supported boundary conditions, and the phenomenon mainly due to the clamped boundary conditions better constrained than the simply supported boundary conditions.

https://doi.org/10.1017/jmech.2012.139 Published online by Cambridge University Press

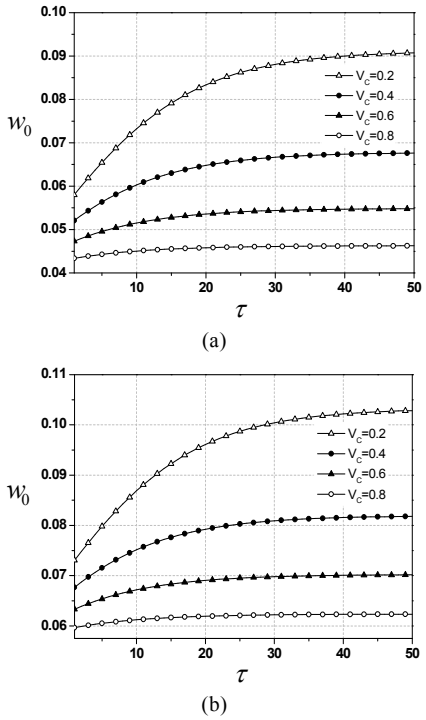


Fig. 3 The change of the center deflection w_0 for the FGM circular plate with different V_c, where $h / a = 0.1$ and $q = 100 \times 10^6 Pa$, (a) the clamped boundary conditions, (b) the simply supported boundary conditions

Figure 4 shows the change of the center deflection for the FGM circular plate with different volume fraction indexes n at the clamped and simply supported boundary conditions. It is seen easily from Fig. 4 that the magnitudes of the center deflection for the FGM circular plate increases as the n increases. Comparing Fig. 4 with Fig. 3, it is seen easily that the change of the center deflection for the FGM circular plate is similar, the magnitude of the deflection in Fig. 4 is smaller than that of in Fig. 3 at the initial time, and the change of the deflection's magnitude in Fig. 4 is larger than that of Fig. 3 as the time increases.

Figure 5 shows the change of the center deflections for the FGM circular plate with different h / a at the clamped and simply supported boundary conditions. From Figs. 5(a) and 5(b), it is seen easily that the changes of the center deflection's magnitude are very small as the time increases, and the magnitude of the center deflections of the FGM circular plate increase as h / a decreases.

4.3 Dynamic Response of the Clamped Viscoelastic FGM Circular Plate

In this section, consider dynamic response of a clamped FGM circular plate, the same material parameters are selected as the section 4.2.

Figures 6(a) and 6(b) show, respectively, the radial stress σ_r and circumferential stress σ_θ of the clamped FGM circular plate with different volume fractions of the ceramic V_c, where $h / a = 0.1$, $\tau = 25s$ and $q = 100$MPa. From Fig. 6(a), it is seen easily that the

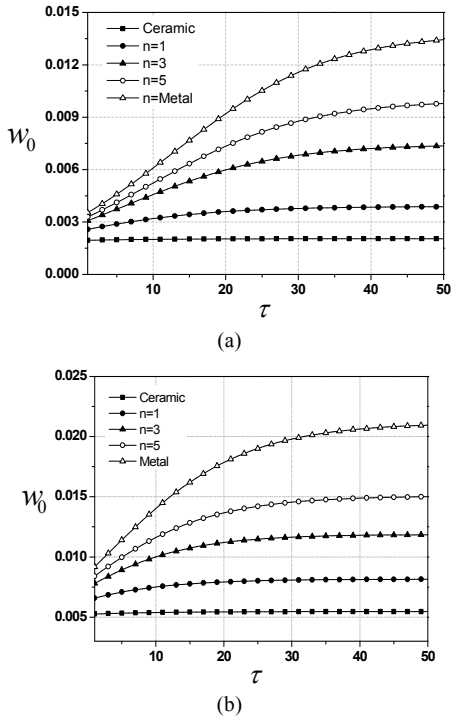


Fig. 4 The change of the center deflection w_0 of the FGM circular plate with different n, where $h / a = 0.1$ and $q = 100 \times 10^6 Pa$, (a) the clamped boundary conditions, (b) the simply supported boundary conditions

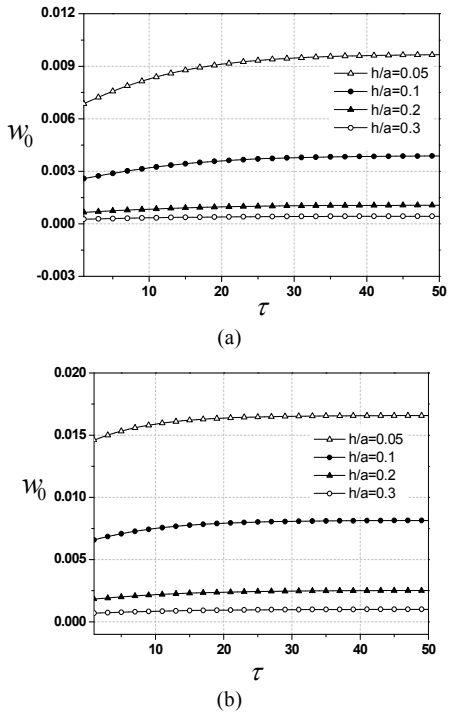


Fig. 5 The change of the center deflection w_0 for the FGM circular plate with different h / a, where $n = 1$ and $q = 100 \times 10^6 Pa$, (a) the clamped boundary conditions, (b) the simply supported boundary conditions

https://doi.org/10.1017/jmech.2012.139 Published online by Cambridge University Press

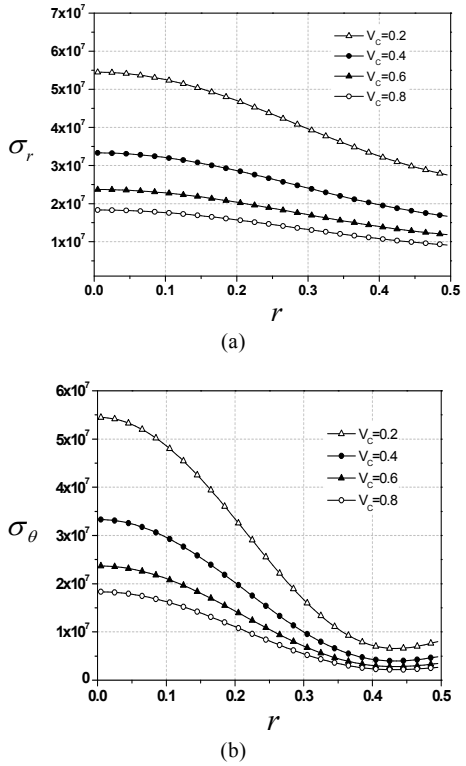


Fig. 6 Stresses of the clamped FGM circular plate with different V_c, where $h / a = 0.1$, $t = 25s$ and $q = 100 \times 10^6 Pa$, (a) the radial stress σ_r, (b) the circumferential stress σ_θ

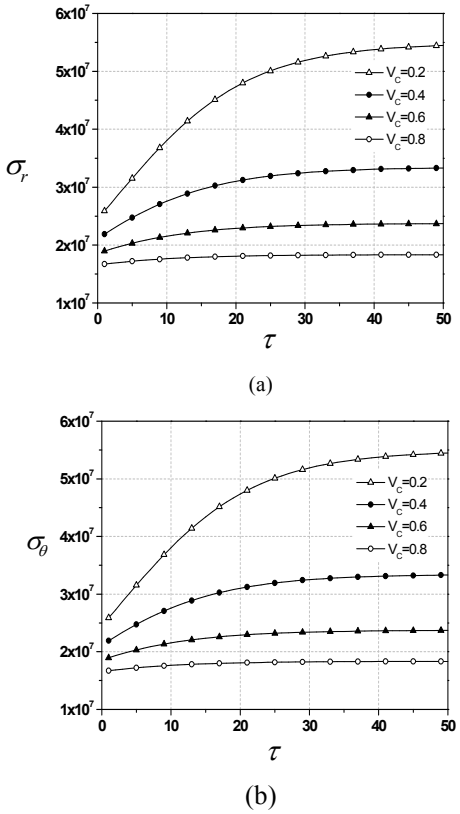


Fig. 7 The center stresses for the clamped FGM circular plate with different V_c, where $h / a = 0.1$ and $q = 100 \times 10^6 Pa$, (a) the center radial stress σ_r, (b) the center circumferential stress σ_θ

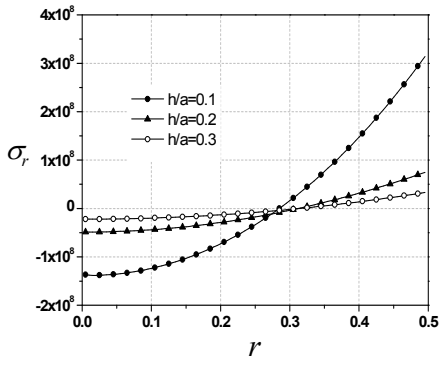
radial stresses decrease with different V_c from the center to the boundary due to the clamped boundary conditions, the magnitude of the radial stress σ_r decreases as V_c increases at the same radial point. The main reason why the stiffness of the FGM circular plate reduces as the volume fractions of the ceramic V_c increases, and the phenomenon shows that the V_c have a great effect on the radial stress of the clamped FGM circular plate. Comparing Fig. 6(b) with Fig. 6(a), it is found that the change trend is similar, the amplitudes of the circumferential stress σ_θ is smaller at the boundaries of the FGM circular plate than those of the radial stress σ_r, and the phenomenon shows the clamped boundary has a great effect on the stress's amplitude at the boundaries of the FGM circular plate.

Figures 7(a) and 7(b) show, respectively, the change of the central radial stress σ_r and circumferential stress σ_θ of the clamped FGM circular plate with different volume fractions of the ceramic V_c as the time τ increases, where $h / a = 0.1$ and $q = 100$MPa. From Fig. 7(a), it is seen that the central radial stresses increase with different V_c as the time τ increases, the magnitude of the central radial stress σ_r decreases as V_c increases at the same time. The main reason why the stiffness of the FGM circular plate becomes low as the volume fractions of the ceramic V_c increases, and the phenomenon denotes the V_c have a great effect on the central radial stress of the clamped FGM circular plate. Comparing Fig. 7(b) with Fig. 7(a), it is found easily that the change trend is similar, and it's magnitude is almost the same.

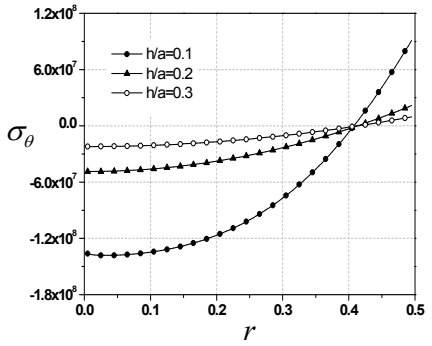
Figures 8(a) and 8(b) depict, respectively, the radial stress σ_r and circumferential stress σ_θ of the clamped FGM circular plate with various h / a, where $n = 1$, $\tau = 25s$ and $q = 100$MPa. It is seen easily from Fig. 8(a) that the radial stresses increase with different h / a as r increases, the magnitude of the radial stress for the clamped viscoelastic FGM circular plate decreases as the ratio of thickness to radius h / a increases, the radial stress' magnitude become smaller due to the FGM circular plate becomes thicker, and the radial stress of the FGM circular plate with different h / a appears equal at the $r = 0.28$. The main reason why the equivalent radial stresses happen at $r = 0.28$ with different h / a is influenced by the clamped boundary and the volume fractions of the ceramic V_c, and the phenomenon shows that the ratio of thickness to radius h / a has a great effect on the radial stress of the clamped FGM circular plate. Comparing Fig. 8(b) with Fig. 8(a), it is seen that the change trend of the circumferential stress is similar as the change trend of radial stress, then the circumferential stress is equal at the $r = 0.41$.

Figures 9(a) and 9(b) depict, respectively, the radial stress σ_r and circumferential stress σ_θ of the clamped FGM circular plate with various mechanical loads q, where $n = 1$, $\tau = 25s$ and $h / a = 0.1$. From Fig. 9(a), it is seen that the radial stresses increase with different q from the center to the boundary, the phenomenon appear due to the clamped boundary conditions. It is also seen from the figure that the magnitude of the

https://doi.org/10.1017/jmech.2012.139 Published online by Cambridge University Press

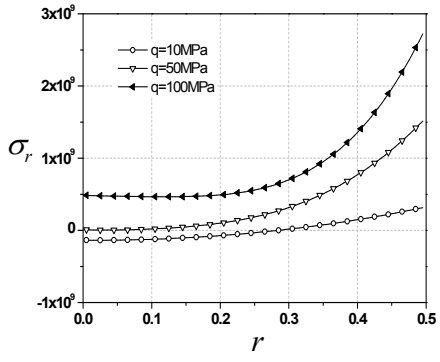


(a)

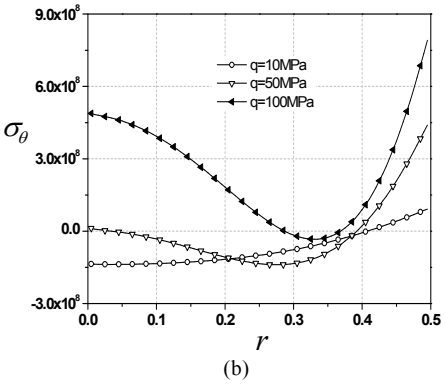


(b)

Fig. 8 Stresses of the clamped FGM circular plate with different h / a, where n = 1, t = 25s and $q = 100 \times 10^6 Pa$, (a) the radial stress σ_r, (b) the circumferential stress σ_θ



(a)



(b)

Fig. 9 Stresses of the clamped FGM circular plate with different q, where n = 1, t = 25s and h / a = 0.1, (a) the radial stress σ_r, (b) the circumferential stress σ_θ

radial stress σ_r increases as the mechanical load q increases at the same radial point. Comparing Fig. 9(b) with Fig. 9(a), the change trend of the circumferential stress is different with the change trend of the radial stress. From Fig. 9(b), when the mechanical load q is less than a certain value, the circumferential stress increases as r increases; when the mechanical load q is more than a certain value, the circumferential stress first decreases and then increases from the center to the boundary. The phenomenon shows that the mechanical load q has a great effect on the circumferential stress of the clamped FGM circular plate.

4. CONCLUSIONS

1. Based on the first-order shear deformation and geometric nonlinear theory, nonlinear dynamic analysis for a FGM circular plate under mechanical load is investigated by adopting the Boltzmann linear superposition principle.
2. Numerical results show that the volume fraction index, boundary conditions, mechanical load and the ratio of thickness to radius have a great influence on dynamic behavior of the FGM circular plate. Therefore, by selecting a proper value of the volume fraction index, engineers can design a specific FGM circular plate that can meet engineering requirements.

ACKNOWLEDGEMENTS

The authors wish to thank reviewers for their valuable comments and the funded by the National Natural Science Foundation of China (Grant No.11072077), State key Laboratory of Advanced Design and Manufacturing for Vehicle Body (Grant No.51075003), and the central colleges of basic scientific research and operational costs (funded by the Hunan University).

REFERENCES

1. Ma, L. S. and Wang, T. J., "Nonlinear Bending and Post-Buckling of a Functionally Graded Circular Plate Under Mechanical and Thermal Loadings," *International Journal of Solids and Structures*, **40**, pp. 3311–3330 (2003).
2. Najafizadeh, M. M. and Eslami, M. R., "Buckling Analysis of Circular Plates of Functionally Graded Materials Under Uniform Radial Compression," *International Journal of Mechanical Sciences*, **44**, pp. 2479–2493 (2002).
3. Najafizadeh, M. M. and Heydari, H. R., "Thermal Buckling of Functionally Graded Circular Plates Based on Higher Order Shear Deformation Plate Theory," *European Journal of Mechanics-A/ Solids*,

https://doi.org/10.1017/jmech.2012.139 Published online by Cambridge University Press

23, pp. 1085–1100 (2004).

4. Ebrahimi, F. and Rastgo, A., "An Analytical Study on the Free Vibration of Smart Circular Thin FGM Plate Based on Classical Plate Theory," *Thin-Walled Structures*, **46**, pp. 1402–1408 (2008).
5. Li, X. Y., Ding, H. J. and Chen, W. Q., "Elasticity Solutions for a Transversely Isotropic Functionally Graded Circular Plate Subjected to an Axisymmetric Transverse Load," *International Journal of Solids and Structures*, **45**, pp. 191–210 (2008).
6. Saidi, A. R., Rasouli, A. and Sahraee, S., "Axisymmetric Bending and Buckling Analysis of Thick Functionally Graded Circular Plates Using Unconstrained Third-Order Shear Deformation Plate Theory," *Composite Structures*, **89**, pp. 110–119 (2009).
7. Hosseini-Hashemi, S. H., Akhavan, H., Rokni Damavandi Taher, H., Daemi, N. and Alibeigloo, A., "Differential Quadrature Analysis of Functionally Graded Circular Sector Plates on Elastic Foundation," *Materials & Design*, **31**, pp. 1871–1880 (2010).
8. Nie, G. J. and Zhong, Z., "Dynamic Analysis of Multi-Directional Functionally Graded Annular Plates," *Applied Mathematical Modelling*, **34**, pp. 608–616 (2010).
9. Ebrahimi, F. and Rastgoo, A., "Nonlinear Vibration Analysis of Piezothermoelectrically Actuated Functionally Graded Circular Plates," *Archive of Applied Mechanics*, **81**, pp. 361–383 (2011).
10. Shariyat, M. and Alipour, M. M., "Differential Transform Vibration and Modal Stress Analyses of Circular Plates Made of Two-Directional Functionally Graded Materials Resting on Elastic Foundations," *Archive of Applied Mechanics*, **81**, pp. 1289–1306 (2011).
11. Shariyat, M. and Jafari, R., "Nonlinear Low-Velocity Impact Response Analysis of a Radially Preloaded Two- Directional-Functionally Graded Circular Plate: A Refined Contact Stiffness Approach," *Composites, Part B: Engineering*, http://dx.doi.org/10.1016/j.compositesb.2012.05.014 (2012).
12. Khorshidvand, A. R., Jabbari, M. and Eslami, M. R., "Thermoelastic Buckling Analysis of Functionally Graded Circular Plates Integrated with Piezoelectric Layers," *Journal of Thermal Stresses*, **35**, pp. 695–717 (2012).
13. Li, X. Y., Li, P. D., Kang, G. Z. and Pan, D. Z., "Axisymmetric Thermoelasticity Field in a Functionally Graded Circular Plate of Transversely Isotropic Material," *Mathematics and Mechanics of Solids*, DOI: 10.1177/1081286512442437 (2012).
14. Woo, J. and Meguid, S. A., "Nonlinear Analysis of Functionally Graded Plates and Shallow Shells," *International Journal of Solids and Structures*, **38**, pp. 7409–7421 (2001).
15. Reddy, J. N., "Analysis of Functionally Graded Plates," *International Journal for Numerical Methods in Engineering*, **47**, pp. 663–684 (2000).
16. Reddy, J. N. and Huang, C. L., "Nonlinear Axisymmetric Bending of Annular Plates with Varying Thickness," *International Journal of Solids and Structures*, **17**, pp. 811–825 (1981).
17. Reddy, J. N., Wang, C. M. and Kitipornchai, S., "Axisymmetric Bending of Functionally Graded Circular and Annular Plates," *European Journal of Mechanics A/Solids*, **18**, pp. 185–199 (1999).
18. Bayat, M., Saleemb, M., Sahari, B. B., Hamoude, A. M. S. and Mahdi, E., "Thermoelastic Analysis of a Functionally Graded Rotating Disk with Small and Large Deflections," *Thin-Walled Structures*, **45**, pp. 677–691 (2007).
19. Fu, Y. M., Li, P. E. and Zheng, Y. F., "Creep Postbuckling of Viscoelastic Plates with Matrix Transverse Cracks," *Acta Mechanica Sinica*. **37**, pp. 32–39 (2005).

(Manuscript received May 2, 2012,
accepted for publication August 17, 2012.)

https://doi.org/10.1017/jmech.2012.139 Published online by Cambridge University Press